

Electron binding and stability of excess-electron alkali halide clusters: Localization and surface states

Eric C. Honea,* Margie L. Homer, and Robert L. Whetten

*Solid State Science Center and Department of Chemistry and Biochemistry, University of California,
Los Angeles, California 90024-1569*

(Received 12 October 1992)

Metal-excess alkali halide clusters have been investigated experimentally using a cluster-beam source comprised of laser ablation of alkali metal and reaction of helium-seeded halogen gas. Metal-excess neutrals and charged clusters, $M_n X_m^{(+)}$ where $M = \text{Na}$ or Li and $X = \text{F}$, Cl , or Br , have been produced, with the neutral series, $M_n X_{n-1}$, displaying a wide range of excess-electron-dominated behavior. An extensive investigation of the abundances and electronic properties of $\text{Na}_n \text{F}_{n-1}$ ($n < 100$) is described. A simple quantitative model of electron localization is proposed to account for the observed patterns of abundances and electron binding energies. The model correctly predicts that (i) for the singular values of n that correspond to a filled cubic lattice, the excess electron is very weakly bound, and that (ii) clusters that can form a cubic lattice with a single anion vacancy have the electron localized in the vacancy, stabilizing the neutral cluster against atom loss.

I. INTRODUCTION

The investigation of finite-size systems—atomic and molecular clusters—provides opportunities to obtain microscopic insight into the properties of a great variety of macroscopic systems as well as the change to explore phenomena intrinsic to finite and interfacial systems.^{1–3} Within this general framework, one very stimulating area of research has been the study of the electronic states and structural properties of the simplest metallic and insulator systems, which represent two extrema along a continuum of condensed-matter phenomena. In bulk metals, the conduction electrons are completely delocalized, and close-packed structures prevail. In insulators, by contrast, an excess electron will remain in a delocalized state only if the crystal symmetry is artificially maintained. In reality, the polarization energy gained by localization about a lattice site offsets the cost of the lattice defect introduced and the increased kinetic energy of the electron. In such solvated-electron systems the spatial extent of the electron wave function, therefore, is rarely more than a few lattice constants, and ground-state transport takes place through either polaron or hopping motions. However, as the excess-electron density is increased from infinite dilution, the correlation among the excess electrons increases, and favors the metallic state above some critical density. Such metal-insulator (MI) transitions remain of high current interest.⁴

In the finite analogs of these systems, the interesting phenomena may be modified in very important ways. In metal clusters, the extent of delocalization is restricted to the physical dimensions of the cluster, and its shape governs the quantization of the electron motion. Still, recent experiment and theory are consistent with the idea that clusters of high-conductivity metals have maximally delocalized valence electrons and compact structures, despite the intrinsic disorder introduced by the cluster surface and the typically nonideal number of atoms for

completing microlattice structures. The electronic shell structure found in clusters of Na demonstrates that to a first approximation, the valence electrons are completely delocalized in a nearly spherical background of ions.⁵ Similar behavior has been observed in metal-rich ionic clusters of $\text{Na}_n \text{Cl}_m$ and $\text{Cs}_n \text{O}_m$ when $m \gg n$, where the number of electrons filling a shell is reduced by the number transferred to the Cl^- or O^{2-} ions.^{6,7}

At the other extreme, the behavior of a single excess electron in finite insulator systems has attracted a great deal of theoretical interest because of the recently developed capability to treat quantum systems at finite temperatures, even with significant symmetry breaking. Several of these classes of systems continue to be central to particular fields of chemistry and condensed-matter physics, including the solvated electron $e-(\text{H}_2\text{O})$,⁸ $e-(\text{NH}_3)$,⁹ e -rare-gas systems (rare gas = He, Kr, Xe),¹⁰ and electrons in alkali halide clusters (e -AHC's).^{11–13} This situation has stimulated the development of a vibrant subfield concerned with the accurate description of their behavior. Although these systems are not nearly so well explored as, for example, the alkali metal clusters, the emerging consensus from recent simulations is that electron localization, accompanied by large-scale structural symmetry breaking in the vicinity of the electron, is as ubiquitous in these clusters as in the bulk, but with important differences. For example, there may exist states in which electrons are localized within the cluster's surface layer, or which spill out onto a close-packed surface. Furthermore, the theoretical simulations almost always employ some kind of simplifying "rigidity" approximations in describing the electron-ion or electron-molecule interactions. Recently, an increasing number of experimental reports have begun to appear,¹⁴ and these provide stringent tests of the conclusions obtained in simulations.^{8–13} In this vein, we have published brief reports on the properties of a crucial model system, the alkali halide clusters containing a single excess elec-

tron.^{12,15-18} This paper presents a full report of our experiments on the electron binding and abundances of this class of clusters.

The starting point for contemplating the properties of the *e*-AHC systems are the alkali halide clusters themselves. Starting in the late 1970s (matrix isolation¹⁹ and simulation²⁰) and early 1980s (mass spectrometry and related cluster-beam methods)²¹⁻²⁵, the alkali halide clusters have been the subject of extensive experimental and theoretical investigation. An important early step was the demonstration by Campana *et al.*²² that the most stable clusters of the form $\text{Cs}(\text{CsI})_n^+$ are those which correspond to filled simple-cubic lattice structures. These can be predicted by the very simple rule $2n + 1 = j \times k \times l$, where the significance of the integers (j, k, l) is that they are the number of ions along one edge of the cluster. Because an odd product of three integers requires all to be odd, this lattice-filling condition is only satisfied for this system when (j, k, l) are all odd; these are $\text{Cs}_{14}\text{I}_{13}^+$ (3,3,3), $\text{Cs}_{23}\text{I}_{22}^+$ (3,3,5), $\text{Cs}_{38}\text{I}_{37}^+$ (3,5,5), It was subsequently shown that the observed abundance ledges result from evaporation of hot clusters generated by sputtering.^{23,24} The microscopic factors underlying the stability of filled lattices is easily understood, and have been elucidated in some detail for clusters of the form $M_n X_m^{n-m}$, where $n - m = -1, 0, 1, 2$ is the excess charge on the cluster.²⁰⁻²⁶ These clusters are regarded as being composed of $n M^+$ ions, $m X^-$ ions, with no excess electrons or neutral atoms that would necessitate a quantum-mechanical treatment. Here we refer to such clusters as "stoichiometric." Subsequent experimental work has been interpreted as being consistent with this principle, that the energy of the cubic lattice is the driving force for stability in stoichiometric AHC's.

The chemical formulas for an *e*-AHC cluster with p excess electrons can be written as $M_n X_m^{n-m-p}$. Clearly, this system could equivalently be regarded as a stoichiometric AHC to which has been added p neutral alkali atoms. When p is small compared to n or m , this is analogous to the bulk situation of low-electron density; in both solid and liquid states this means that an electron occupies its own site in an ionic condensed medium. There are four points to keep in mind here: (i) In the solid alkali halides, this so-called *F*-center state has the e^- in place of an X^- ion in the cubic lattice;²⁷ (ii) an analogous state is known to persist in the dilute liquid-metal and/or molten-salt mixtures,²⁸ in which the electron transport is better described as quantum-mechanical hopping, rather than polaron motion;²⁹ (iii) for higher electron densities, e.g., near 0.15 mole fraction in KBr, the system becomes metallic;³⁰ it has been proposed that this phenomenon might be observable in small clusters ($n < 100$), although segregation may be a problem at low cluster temperatures;^{6,7} (iv) in clusters, the electron can also localize in low coordination number, anion-deficient sites in the surface layer or on the surface; such states have recently been characterized successfully for the NaCl(100) crystal surface using atomic force microscopy;³¹ related phenomena have been observed for metal-rich alkaline-earth surfaces.³²

Landman and co-workers used quantum path-integral

Monte Carlo (QPIMC) calculations to describe the state of a single excess electron in AHC's larger than $n = 2$.¹³ In their work, they used parametrized pair potentials for the interior interactions ($\text{Na}^+ - \text{Cl}^-$, $\text{Na}^+ - \text{Na}^+$, and $\text{Cl}^- - \text{Cl}^-$) and simple pseudopotentials for the *e*-ion interactions. Earlier calculations exist for the Na_2Cl molecule's geometry and ionization potential.³³ For larger systems, conventional quantum-chemical techniques become impractical, and the techniques of solid-state theory breakdown due to a lack of periodic symmetry, so one requires new computational methods, such as coupled classical-quantum numerical simulations. In several reports, Landman *et al.* used these methods and described a remarkable range of behavior dominated by the excess electron.¹³ These results formed the basis for three essential predictions.

(i) Attachment of an excess electron to a filled cubic lattice (j, k, l) results in a weakly bound *surface state*, in which the electron localizes about a single-surface Na^+ ion. The e^- cannot displace an interior Cl^- or F^- ion to the surface, but the interaction is strong enough to localize the electron even at low temperatures and distort the cluster from its otherwise high symmetry.

(ii) If the electron can localize in a single anion-deficient site to complete a filled cubic lattice, then it will do so to form a stable cluster. This is strongly reminiscent of the localization which forms the *F*-center state in bulk alkali halides, although the electron's environment is far from cubic in the surface-layer states that are usually found to be most stable. And even when it does localize in the interior, the long-range aspect of the Coulomb potential may make this state quantitatively quite different. This type of localization was found in clusters with the charge states $-1, 0$, and $+1$.

(iii) The characteristic decay mode of the *e*-AHC system is a Na^0 atom loss, a process that can be viewed as occurring in two stages: At elevated temperatures, a fluctuation causes a Na^+ ion to be effectively neutralized by the e^- ; this atom, unable to participate in the ionic bonding of the lattice, subsequently detaches from the cluster.

Another process that may be of some interest is that of *electron-attachment-induced isomerization*. Attachment of an e^- to a tetrahedral Na_4Cl_4 cluster at low temperatures causes it to open up into a quasiplanar 3×3 structure, with the e^- occupying a chloride-deficient site.

Along with these general findings, the QPIMC simulations generate a great deal of quantitative information, some of which, such as electron binding energies (vertical and adiabatic) can be compared directly to experiment.

In our recent Letter¹⁵ on the *e*-AHC system $\text{Na}_n \text{F}_{n-1}$ ($n < 100$), we reported evidence to support all three of these rules, along with the corollary to (i) and (ii) that those clusters that do fail to satisfy either (i) $2n - 1 = j \times k \times l$ or (ii) $2n = j \times k \times l$ are particularly unstable with respect to process (iii), atom detachment, and therefore are observed in relatively low abundance. In this full report, we present abundances of neutral $\text{Na}_n \text{Cl}_{n-1}$, $\text{Na}_n \text{F}_{n-1}$, and $\text{Li}_n \text{F}_{n-1}$ clusters, and charged $\text{Na}_n \text{F}_{n-1}^+$ and $\text{Na}_n \text{F}_{n-2}^+$. Photoionization spectroscopy has been used to obtain electron binding energies and information about neutral-to-ion cluster reorganization

energies. Monte Carlo simulations of Na_nF_n and $\text{Na}_n\text{F}_{n-1}^+$ clusters (without excess electrons) were performed to provide insight into the geometries and energies of the excess-electron clusters. Some of the lowest-energy structures are presented here, and the rest are presented in a separate paper.³⁴ Where possible, we compare our results to theoretical predictions. A simple quantitative model, in which the excess electron is localized and substitutes for an anion, is used to describe the observed cluster abundances and electron binding energies.

II. EXPERIMENTAL METHODS

A. Apparatus

The experimental apparatus is shown in Fig. 1. The clusters are produced in a pulsed-jet laser vaporization source. Upon expansion into a vacuum, the jet is

skimmed as it passes through a differentially pumped region before entering the acceleration field of a Wiley-McLaren time-of-flight mass spectrometer. The clusters are ionized either by fixed-wavelength (248, 308 nm) excimer lasers or the fundamental or second harmonic of a tunable dye laser.

Charged clusters generated concurrently in the source are analyzed using pulsed acceleration fields in the time-of-flight mass spectrometer. Both on-axis and perpendicular ion extraction [as in Fig. 1(a)] were used. Perpendicular extraction results in better mass resolution at the expense of lower signal levels.

B. Cluster Source

The laser vaporization source is similar to a type described previously,³⁵ with some modifications made for

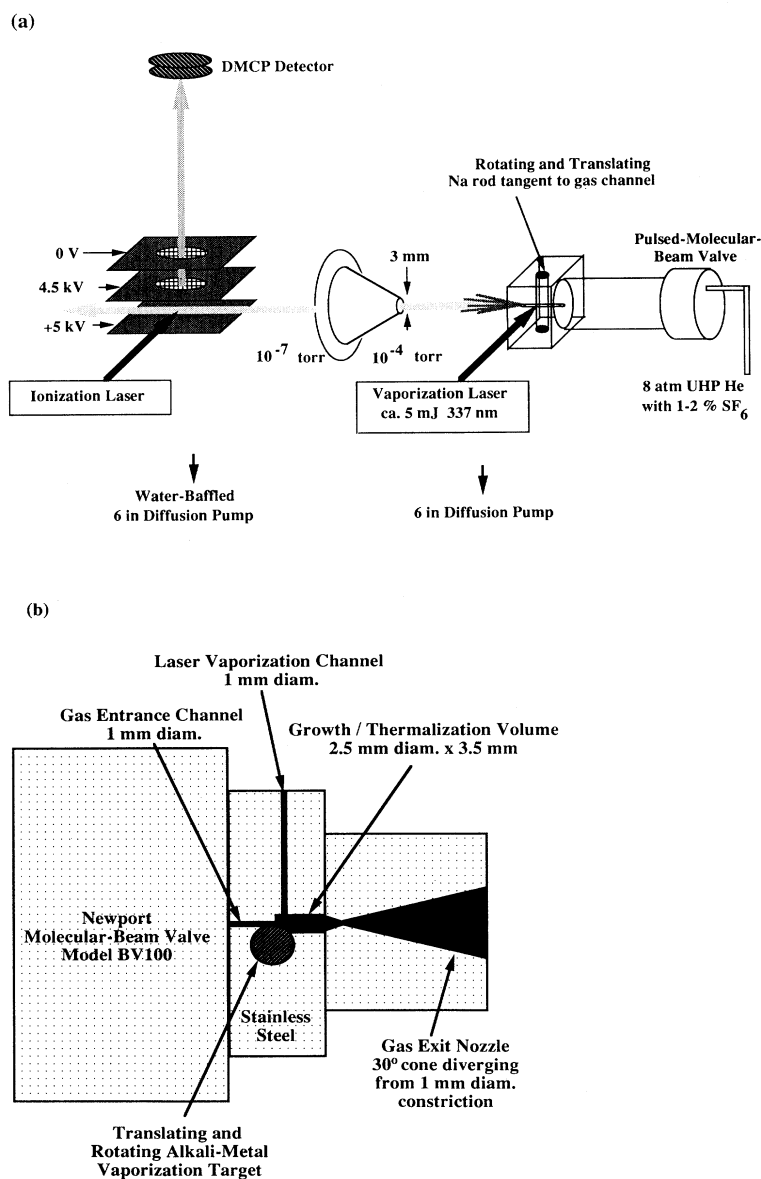


FIG. 1. (a) Schematic of experimental apparatus used for production and photoionization of neutral M_nX_m clusters. The clusters are formed by uv laser vaporization of an alkali metal rod into a halogen-seeded He flow stream. The pulsed jet is skimmed and the cluster ions (formed by photoionization or taken directly from the vaporization source) are accelerated in a Wiley-McLaren time-of-flight mass spectrometer. The cluster ions are separated in time during the 50-cm field-free drift region and strike a dual microchannel plate detector. Mass spectra are recorded with a personal computer controlled 100-MHz transient digitizer. Some of the experiments were performed with the time-of-flight mass spectrometer in an additional turbomolecular pumped chamber at $< 10^{-7}$ torr. Positive ions from the source were detected with the mass spectrometer on axis and a pulsed voltage applied to the acceleration plates. (b) Detail of the alkali halide vaporization source.

the use of alkali metals [Fig. 1(b)]. A plastic glove bag is attached to the source chamber to fabricate the alkali metal target rod in an inert atmosphere each time the experiment is run. After purging both the chamber and glove bag with argon, a fresh sodium rod is formed by forcing a thin wall tube of the appropriate diameter into a solid block of the soft metal (99.9%) to slice a smooth-surfaced sample. In the case of lithium, the rod is formed by forcing nominal 1/8-in. outer diameter wire (99.9%) into the same tube. In order to hold the rod securely, a hole is manually drilled through the rod center so that a stainless-steel screw can be inserted. The rod-screw assembly is attached by the screw to a threaded holder, which serves to rotate and translate the rod as it is laser vaporized.

This same procedure is also used in our source³⁶ of alkali atomic clusters (Na_n , Li_n), except that for all alkali atomics the nozzle is shaped for greater flow restriction and the entire rod-nozzle assembly is cooled to cryogenic temperatures.

In order to form the alkali halide clusters, a small amount (ca. 1% partial pressure) of halogen-containing molecule is seeded into the He (99.999% purity) carrier gas. If no halogen is introduced, background H_2O vapor is the major surface contaminant and leads to sodium-hydroxide clusters of the form $\text{Na}_n(\text{OH})_m$. For Na_nCl_m , the He buffer gas was bubbled through CCl_4 or SnCl_4 at temperatures varied to control stoichiometry. Similarly, the convenient vapor pressure of CH_2Br_2 was used for Na_nBr_m , though complexes with nonalkali halide constituents congested the mass spectra. The most convenient and stable alkali halide cluster production was that of Na_nF_m and Li_nF_m , where SF_6 was mixed with He in various concentrations.

Very modest pulse energies are found to be sufficient for efficient target vaporization and cluster production. A N_2 laser (337 nm, approximately 5 mJ) focused with a 20-cm lens was used for vaporization. Photolysis of the halogen-containing molecule is the source of halide for the clusters; when halogen-containing molecules are introduced downstream of the sodium vapor, only metal (or "dirty" metal) clusters are produced. Also, there is some evidence that the ambient surface has a metal halide overlayer. If we switch halogen-containing seed gases while using the same rod, the source produces clusters containing both halides; this result is only temporary and after several passes on the rod, the clusters only contain the halide from the new seed gas.

Considerable effort has been devoted to improving the stability and reproducibility of this kind of source. However, the probability of success in generating a stable beam has never been much above 50%, so that further measures are usually needed to obtain precise results (see below).

C. Photoionization mass spectrometry

Photoionization mass spectra are obtained at a fixed photon energy by directing the spatially filtered radiation from the dye-laser or excimer-laser sources into the acceleration region of the time-of-flight mass spectrometer.

The fluence is determined from the transmitted beam area and the pulse energy as measured by a pyroelectric detector, and can be controlled over a large range using neutral-density filters. Photoionization spectra are generated by scanning the laser over a dye range, either in large steps (in which case mass spectra are recorded at each wavelength and stored for further analysis) or in fine increments, in which case only the integrated intensity of the mass spectral peaks are stored in the form of a mass-energy array, using a data-acquisition program developed earlier.

In the case of continuous scans of this latter type, it has also been found to be desirable to have a means of internal normalization of the signal, in order to remove the effect of fluctuating or drifting cluster-beam intensity. This procedure is described in full in our paper on photoionization spectroscopy of alkali clusters.³⁷ Here we note simply that a third laser (KrF, 5.0 eV) is time delayed (10^{-7} s) and slightly displaced spatially from the dye-laser pulse, providing a reference mass spectral peak arriving slightly after each dye-laser-generated cluster peak.

III. EXPERIMENTAL RESULTS AND ANALYSIS

A. Beam composition from charged-cluster (Na_nF_m^+) abundances

The simplest experiment that can be performed is to measure the relative abundance of charged clusters generated directly in the source. This also permits some comparison to earlier experiments which usually detected only charged-cluster stability. Figure 2 shows a mass spectrum of Na_nF_m^+ cluster ions produced directly in the vaporization source and mass analyzed *without* an additional ionization process. The main series is $\text{Na}_n\text{F}_{n-1}^+$, with the special sizes $\text{Na}_{14}\text{F}_{13}^+$, $\text{Na}_{23}\text{F}_{22}^+$, and $\text{Na}_{38}\text{F}_{37}^+$ displaying enhanced stability. These "magic numbers" are the same as those found in previous studies of sputtered ions, high-energy electron-impact ionization of $(\text{NaCl})_n$ clusters produced in a gas aggregation source,²⁵ and direct laser vaporization of solid NaCl into an expanding jet of helium or argon gas.³⁸ As found

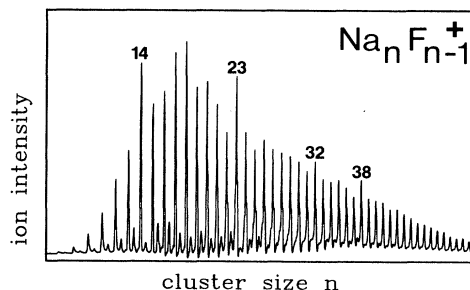


FIG. 2. Mass spectrum of $\text{Na}_n\text{F}_{n-1}^+$ and $\text{Na}_n\text{F}_{n-2}^+$ cluster ions obtained under metal-rich conditions. The $\text{Na}_n\text{F}_{n-1}^+$ clusters (main series) show enhanced relative stabilities for cubic cluster ions such as $\text{Na}_{14}\text{F}_{13}^+$ (a $3 \times 3 \times 3$ cube) and $\text{Na}_{23}\text{F}_{22}^+$ (a $3 \times 3 \times 5$ cuboid). The excess-electron $\text{Na}_n\text{F}_{n-2}^+$ clusters (minor series) also show enhanced stability for the $\text{Na}_{14}\text{F}_{12}^+$ and $\text{Na}_{23}\text{F}_{21}^+$ (not completely resolved) clusters suggesting that the excess electron is localized in the anion vacancy.

in our Monte Carlo simulations³⁴ and discussed in the Introduction, the enhanced stability of these sizes has been attributed to cubic structures that can be formed with an odd number of lattice sites, such as the $3 \times 3 \times 3$ $\text{Na}_{14}\text{F}_{13}^+$. The fine structure in the abundances is consistent with previous observations of surface steps on incomplete cuboid lattices.³⁸

In addition to this well-established pattern, the additional series $\text{Na}_n\text{F}_{n-2}^+$ (excess electron) and Na_nF_n^+ (excess hole), are found with appropriate halogen concentration and source conditions. We have discussed these in detail in a recent paper devoted to charged clusters.¹⁶

The relative abundance of stoichiometric to excess-electron clusters shows that under the conditions used to study the single-excess-electron clusters, the stoichiometric clusters form the major part of the beam. When all charged clusters are detected, as in Fig. 2, the various steps may overlap and complicate assignment of properties to a given cluster stoichiometry and size. As discussed below, in the study of the neutral clusters an appropriate choice of photoionization energy allows one to ionize and detect only the excess-electron species due to their significantly lower ionization potentials.

B. Neutral cluster abundances by photoionization mass spectrometry

A typical photoionization mass spectrum of neutral $\text{Na}_n\text{F}_{n-1}$ clusters, obtained with relatively low fluence (ca. 1 mJ/cm^2) and 5.0-eV photons, is shown in Fig. 3. Comparison of mass spectra of neutral $\text{Na}_n\text{Cl}_{n-1}$, $\text{Na}_n\text{F}_{n-1}$, and $\text{Li}_n\text{F}_{n-1}$ clusters under similar conditions is shown in Fig. 4. The peaks shown in this figure are believed to represent the actual variation in abundances of the corresponding neutral clusters, for the following reasons: For the $\text{Na}_n\text{F}_{n-1}$ clusters, this pattern was

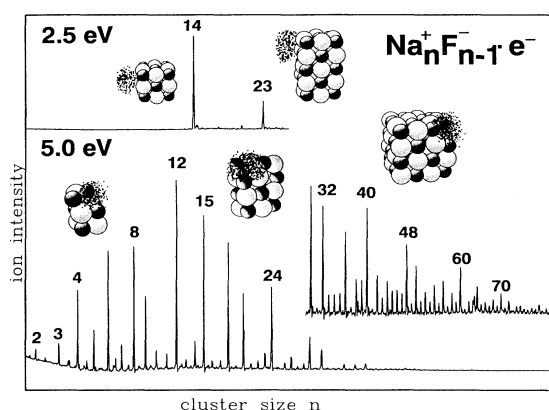


FIG. 3. Photoionization mass spectra of $\text{Na}_n\text{F}_{n-1}$ clusters, $n=2-83$, at $h\nu=5.0 \text{ eV}$ (lower trace) and 2.5 eV (upper). The structures show the hypothetical modes of localization of an electron (dot cloud) around computed $\text{Na}_n\text{F}_{n-1}^+$ structures: (upper) the $n=14$ (3,3,3) and $n=23$ (3,3,5) cuboids, with the electron in a surface state; (lower) the $n=6$ (2,2,3), 12 (2,3,4), and 32 (4,4,4) cuboids with the electron in a surface F-center state (vertex sites).

found to be relatively independent of photon energy in the 5.0–5.6-eV range, and independent of photon fluence in the range 10^{-4} to $10^{-2} \text{ J cm}^{-2}$. This photon fluence is many orders of magnitude below that employed to study multiphoton stimulated desorption of $(\text{NaCl})_n$ clusters from a gas aggregation source.²⁵ Stoichiometric alkali halide clusters such as $(\text{NaF})_n$ are expected to be “transparent” at these photon energies. The abundance pat-

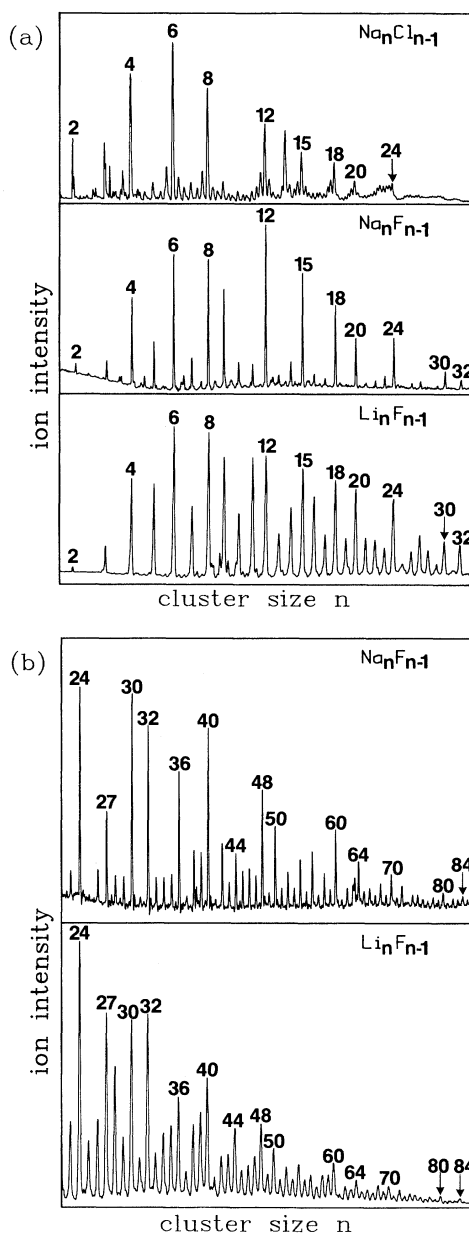


FIG. 4. Mass spectra of neutral excess-electron $M_n X_{n-1}$ clusters obtained with single-photon photoionization at 5.0 eV (KrF laser line). (a) Relative abundances of $\text{Na}_n\text{Cl}_{n-1}$, $\text{Na}_n\text{F}_{n-1}$, and $\text{Li}_n\text{F}_{n-1}$ clusters: mass spectrometer optimized for smaller clusters. (b) $\text{Na}_n\text{F}_{n-1}$ and $\text{Li}_n\text{F}_{n-1}$ clusters: similar to (a) with mass spectrometer optimized for larger clusters and increased signal amplification.

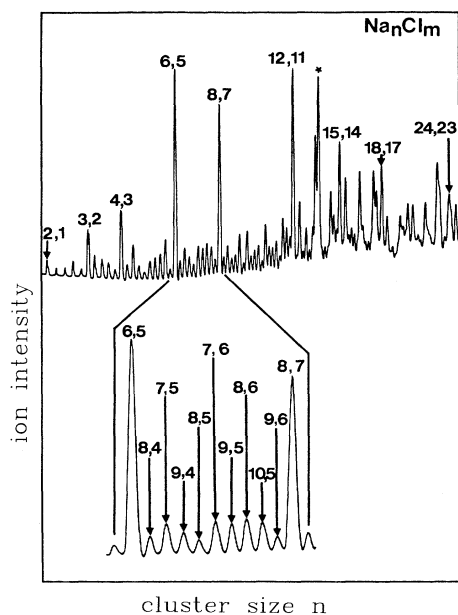


FIG. 5. Mass spectrum of Na_nCl_m neutral clusters detected with 5.0-eV photoionization. The enlargement around 400 amu identifies the multiple excess-electron clusters. Note the overlap of the various series at larger sizes due to the limited mass resolution of the spectrometer. Since CCl_4 is introduced into the He carrier gas to form the alkali halide clusters, carbon is incorporated into some of the clusters: the peak marked with an asterisk corresponds to $\text{Na}_{14}\text{Cl}_{12}\text{C}$ (see Ref. 46).

terns are relatively independent of the choice of halogen (F, Cl, or Br), as might have been expected for ionic bonding. Additionally, this basic pattern is completely different from the $M_nX_{n-1}^+$ mass spectra in Fig. 2, demonstrating that is not simply a consequence of post-ionization fragmentation. The photon energies used here result in the detection of only the excess electron M_nX_{n-1} neutrals, unlike Fig. 2 where the less abundant excess-electron series is obscured by the dominant (stoichiometric) $\text{Na}_n\text{F}_{n-1}^+$ series.

Figure 5 shows a portion of a mass spectrum of Na_nCl_m clusters obtained under metal-rich ($n > m$) conditions. The inset identifies the multiple excess-electron series around 400 amu. The limited mass resolution of our spectrometer and the mass peak broadening, resulting from the natural $^{35}\text{Cl}/^{37}\text{Cl}$ isotopic distribution, make the assignments tentative, but the peak assignments are precise to within 1 amu. As can be seen in the larger masses, the spectrum becomes congested very quickly with increasing size. In addition, carbon (from CCl_4) is incorporated into some cluster sizes and tends to further complicate the mass spectra.³⁹

While the mass spectra in Fig. 3 for the various alkali halide systems are remarkably similar, the mass spectra of $\text{Na}_n(\text{OH})_m$ clusters (not shown), arising from ambient water and obtained with 5.0-eV photoionization, show a dominant $\text{Na}_n(\text{OH})_{n-1}$ series, with enhanced stability for $n=4, 9, 18, 20,$ and 24 . The difference between hydrox-

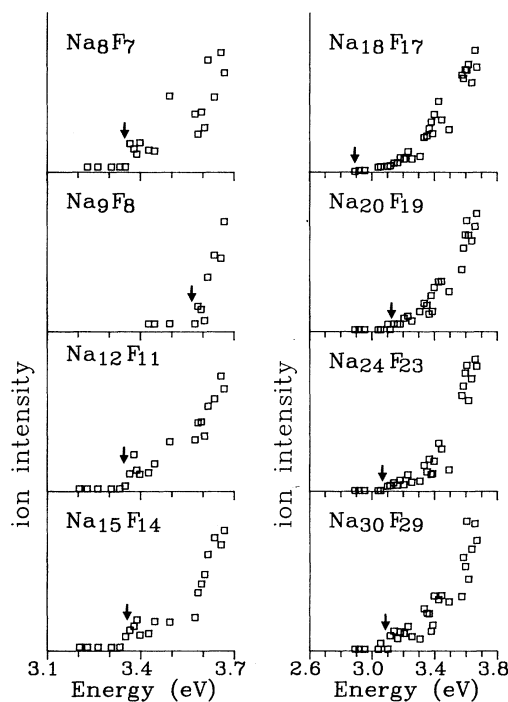


FIG. 6. Photoionization efficiency curves for several $\text{Na}_n\text{F}_{n-1}$ clusters in the 2.8–3.7-eV range, with the assigned thresholds marked. In this case, the signal for each cluster size was normalized to the $\text{Na}_{14}\text{F}_{13}$ or $\text{Na}_{23}\text{F}_{22}$ signals which were assumed constant across this energy range. In order to compare to predicted adiabatic electron binding energies, the threshold was assigned as the intercept of the last decline of the signal.

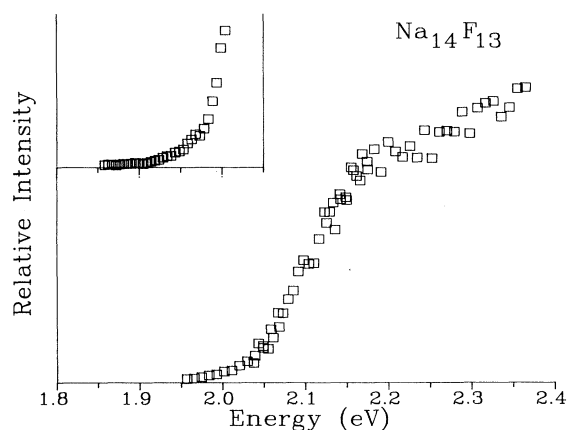


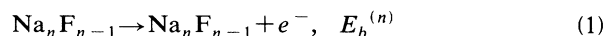
FIG. 7. Photoionization efficiency curve for $\text{Na}_{14}\text{F}_{13}$ between 1.8 and 2.4 eV. The composite curve was obtained from scans of relative intensity across four laser dyes. Normalization from one scan to another was done by linearly scaling one of the scans to match the other in the region of wavelength overlap. The inset shows the last decline of the ion signal between 1.80 and 2.05 eV.

ide and halide magic numbers is evidence of the different lattice structures. In this case, the alkali halide magic numbers are characteristic of cuboid microfragments of the NaCl structure (see below), whereas low-temperature (< 300°C) NaOH assumes different crystal structure from NaCl; the small clusters in this size range do not appear to have the NaCl structure either.

C. Photoionization spectroscopy of $\text{Na}_n\text{F}_{n-1}$ clusters

The binding energy of the excess electron has been determined for many of the $\text{Na}_n\text{F}_{n-1}$ clusters, $n < 33$, by measuring the photoionization threshold energy using continuously tunable radiation in the 1.8–3.7 eV region and fixed energy lines at 4.0 and 5.0 eV. Previously, this quantity was known only for the M_2X dialkali monohalides.⁴⁰ Qualitatively, the observations are the following. (i) Between 5.0 and 4.0 eV, many of the rela-

tively less abundant clusters nearly disappear while the abundant clusters are unaffected. (ii) Below 3.7 eV the ionization thresholds for the most abundant clusters were determined by recording mass spectra with tunable dye laser. (iii) Two clusters, $\text{Na}_{14}\text{F}_{13}$ and $\text{Na}_{23}\text{F}_{22}$, have featureless photoionization spectra in this energy region, and show thresholds only at very low energy, as indicated by the Fig. 3 inset mass spectrum recorded at 2.5 eV. Threshold curves are shown for several clusters in Fig. 6, with the deduced ionization thresholds for the process



displayed as electron binding energies $E_b^{(n)}$. The photoionization spectrum of $\text{Na}_{14}\text{F}_{13}$ over the low-energy range is shown in Fig. 7.

Two factors may affect the analysis and interpretation

TABLE I. Characteristics of $\text{Na}_n\text{F}_{n-1}$ clusters.

$n, n-1$	j, k, l	E_b model ^a	E_b expt	E_f
Class I: Surface electron				
14,13	3,3,3	2.2	1.88±0.05	1.1
23,22	3,3,5		1.80±0.10	
32,31	3×3×7			
38,37	3×5×5			
Class II: Surface <i>F</i> center				
2,1	1,2,2	3.6	3.85±0.15	1.3
3,2	1,2,3	3.8	3.85	1.0
4,3	2,2,2	4.2	3.54±0.05	1.2
6,5	2,2,3	4.0	3.33	1.6
8,7	2,2,4	4.0	3.35	1.5
9,8	2,3,3	3.7	3.57	1.4
12,11	2,3,4	3.8	3.35	1.6
15,14	2,3,5	3.5	3.35	1.6
18,17	3,3,4	3.4	2.89	2.0
20,19	2,4,5		3.13	
24,23	3,4,4		3.07	
27,26	3,3,6			
30,29	3,4,5		3.09	
32,31	4,4,4			
larger				
36,35	3,4,6			
40,39	4,4,5			
42,41	3,4,7			
48,47	4,4,6			
50,49	4,5,5			
60,59	4,5,6			
70,69	4,5,7			
72,71	4,6,6			
80,79	4,5,8			
Class III: Noncubic				
5,4		3.0	3.85±0.15	0.6
7,6		3.4	3.85	0.6
10,9		3.4	3.85	0.8
11,10		3.3	3.80	1.0
13,12		3.0	3.85	0.7
16,15		2.9	3.85	1.2
17,16		2.4		0.6
19,18				

^aFrom Eq. (2).

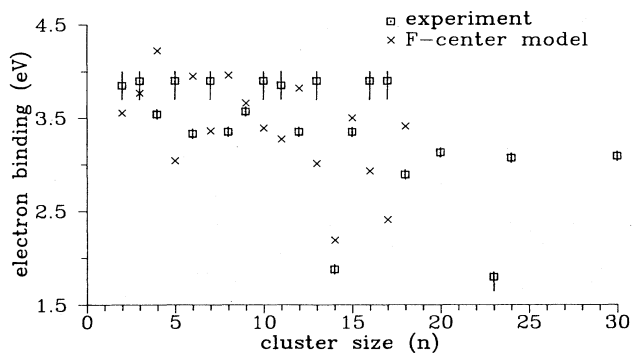


FIG. 8. Comparison of measured and predicted adiabatic binding energies of an excess electron interacting with an $\text{Na}_n\text{F}_{n-1}$ cluster. Note how the binding energies seem to fall into three categories, giving insight into the structure of the clusters.

of the observed thresholds. First, substantial local structural changes can accompany the ionization process in ionic systems (see also below). Second, thermal effects that could round the threshold should be negligible in our experiments, since the jet-cooled clusters are expected to be much colder than room temperature. Unfavorable Franck-Condon factors between the neutral and the charged cluster can result in a broad decline in photoionization efficiency between the vertical and adiabatic ionization energies. In order to obtain adiabatic electron binding energies, thresholds were taken as the zero signal intercept of the last decline of the ion signal. For a finite signal-to-noise ratio, this procedure may overestimate the electron binding energy, depending on the curvature in the threshold region.

The dependence of electron binding energy on cluster size is illustrated in Fig. 8. The most remarkable feature, clearly evident in Fig. 8, is the tendency of a large number of different clusters to have nearly identical electron binding energies: in the 3.8–4.0-eV range, in the 2.9–3.6-eV range, and near 2.0 eV. This distinction is used below to classify the types of clusters as in Table I.

IV. DISCUSSION

A. Background

In the familiar picture of ionic bonding in alkali halide crystals, each metal and halogen atom is in the positive (M^+) and negative (X^-) form of the closed-shell ion. The state of an excess electron reflects both its electrostatic interaction with the ions and the requirement that its wave function is orthogonal to the orbitals of the ion cores. For an electron in an anion vacancy in an infinite crystal, the Coulombic term is sufficiently large to favor a localized ground state in the vacancy. Neglecting a small relaxation of the ions around this site, the Madelung energy is essentially the same as that of the missing anion, and is sufficient to compensate for the increased zero-point energy that arises from localization. These principles may also be applicable to a finite system, or at a surface, except that different electron attachment modes may be energetically preferred. In this respect, the

finite-size clusters explored in this research serve as tractable “microscopic surfaces” and should provide insight into surface states of excess electrons in macroscopic crystals.

Figure 9 shows a schematic energy-level diagram for an excess-electron alkali halide cluster ($e\text{-AHC}$). For a stoichiometric $(\text{NaF})_n$ cluster, the first electronic excitation, from the filled $\text{F}^- (2p)$ band to the empty $\text{Na}^+ (3s)$ band, should require a large energy (near or above 9 eV) as is the case for a NaF thin film.⁴¹ If an electron is substituted for one of the fluoride ions, one state of the $2p$ band is removed in favor of a state in the gap. The excess electron will be bound by significantly lower energy and will display a new excitation spectrum. Experimentally we find that the binding energy of the excess electron is less than the Na ionization potential, and that the spectrum has new states in the 1.2–2.0-eV excitation energy range.

In the quantum path-integral simulation of Landman, Scharf, and Jortner (LSJ), the $\text{Na}_{14}\text{Cl}_{12}^+$ cluster found the electron in an *internal* anion vacancy, in close analogy to an *F* center in a bulk crystal.¹³ The idea that the excess electron can substitute for an anion in an alkali halide cluster does appear to extend to the smallest clusters— Na_2Cl_2 and Na_2Cl have nearly identical rhombic structures if one considers the excess electron in Na_2Cl as substituting for the missing Cl^- ion.⁴² In our earlier report, we presented evidence that many excess-electron alkali halide clusters formed cubic structures with an electron occupying an anion vacancy.¹⁵ For a small cluster, such as Na_4F_3 where the seven ions and the excess electron could be located at the corners of a cube, the electron state could be described as a vacancy in the *surface* layer. The coupled classical-quantum simulations of Rajagopal and co-workers find that this is indeed the case in Na_4F_3 (albeit with the cube distorted and the electron cloud spilling out of the corner site).^{11,12} The charged excess-electron clusters that form cubic structures of high relative stability have also been described as localizing the electron surface-layer states: $\text{Na}_{14}\text{F}_{12}^+$,¹⁶ $\text{Na}_{13}\text{Cl}_{13}^-$,¹⁷ and $\text{K}_{13}\text{I}_{13}^-$.¹⁸

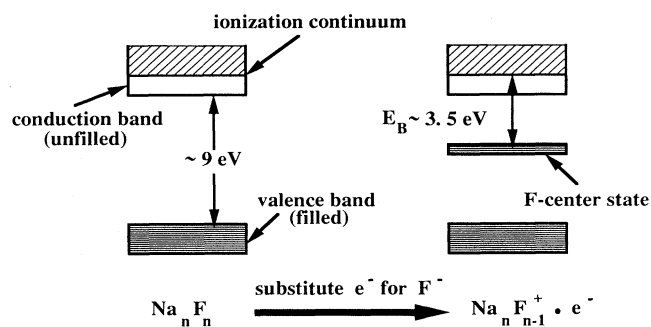


FIG. 9. Band structure of the purely ionic $(\text{NaF})_n$ and excess-electron $\text{Na}_n\text{F}_{n-1}$ clusters. The very large band gap (> 9 eV) for the purely ionic cluster means these clusters are transparent for the photoionization energies used to study the $\text{Na}_n\text{F}_{n-1}$ clusters.

Not in every case does an alkali halide cluster have an obvious anion vacancy for the electron to localize. In the pioneering work of LSJ they also found other types of excess-electron behavior. For instance, an excess electron attached to Na_5Cl_4 tends to neutralize a Na ion, making the cluster unstable toward isomerization and more likely to lose a Na atom. In the experiments, this would be reflected in low abundances of certain clusters.

For the special case of a charged cluster with no inter- or anion vacancy, a different attachment behavior may be expected. For example, for an electron interacting with $\text{Na}_{14}\text{Cl}_{13}^+$, the $3 \times 3 \times 3$ cubic structure (see Fig. 3), the attachment results in some distortion of the cube without displacing an ion from the lattice. The resulting electron binding energy is quite small, ~ 1.5 eV. Landman, Scharf, and Jortner pointed out the analogy between this excess-electron-state and Tamm's crystal surface states.^{13,43}

B. Classification of $\text{Na}_n\text{F}_{n-1}$ clusters

On the basis of the experimentally observed cluster abundances and excess-electron binding energies, and drawing on ideas from the body of theoretical work discussed above, we can classify the excess electron M_nX_{n-1} clusters into three categories. As a specific example, classifications for the $\text{Na}_n\text{F}_{n-1}$ clusters $n=2-80$ are listed in Table I.

Class I. These have the requisite number of ions to form a filled cubic microlattice, $j \times k \times l$ ions on each edge of the cubic lattice. Since the M_nX_{n-1} clusters always have an odd number of ions, this can only occur for $j \times k \times l = 2n - 1$ (i.e., j, k, l all odd). Examples of these clusters are $\text{Na}_{14}\text{F}_{13}$ (3,3,3) and $\text{Na}_{23}\text{F}_{22}$ (3,3,5). These *surface-electron states* are characterized by very low electron binding energies and moderate abundances—they do not fill a cubic lattice, but detaching a neutral atom also fails to produce a cubic lattice.

Class II. A large number of cubic structures other than those of the Class I clusters are possible if the constraint on (j, k, l) is relaxed. Stoichiometric alkali halide clusters such as $(\text{NaF})_n$ take on cuboid structures when the cluster has the correct number of atoms to fill the lattice; in this case $j \times k \times l = 2n$. The M_nX_{n-1} clusters fill $2n - 1$ of the lattice sites, but if the excess electron localizes in the anion vacancy of the M_nX_{n-1} cluster, it can contribute nearly the same potential energy to the cluster as a negatively charged halide ion. The cluster can be regarded as stoichiometric, $M_n^+Y_n^-$, where $Y^- = X^-$ or e^- . We refer loosely to this mode of electron attachment as a *surface F center*, because of the expectation that the electron will localize in the surface layer. We find that these clusters are characterized by enhanced stability (in this case the excess electron stabilizes the cluster against atom loss) and medium electron binding energy, ca. 3.3 eV. Examples are Na_4F_3 (2,2,2) and $\text{Na}_{18}\text{F}_{17}$ (3,3,4).

Class III. For the case where the cluster does not have the requisite number of atoms to satisfy either of the above classes, the clusters are characterized by low abundance, reflecting instability toward Na atom loss, and high electron binding energy. We refer to these clusters

as *noncubic*. Examples are Na_5F_4 and Na_{10}F_9 .

The abundance pattern found for the larger sizes can be discussed in terms of this classification, and in particular with reference to the Class II clusters, at three levels.

(i) The locally major peaks in Figs. 3 and 4 can all be rationalized in terms of the $2n = j \times k \times l$ rule, with all $j, k, l > 2$. The more prominent of these have $j, k,$ and l roughly equal in magnitude. For example, starting with $n = 24$ (3,4,4), one finds 30 (3,4,5), 32 (4,4,4), 36 (3,4,6), 40 (4,4,5), 42 (3,4,7) (although not present in the LiF case), 48 (4,4,6), 50 (4,5,5), 60 (4,5,6), 70 (4,5,7), 72 (4,6,6), 80 (4,5,8), 84 (4,6,7), 90 (4,5,9), 96 (4,6,8), and 100 (5,5,8).

(ii) Clusters of even n tend to be more abundant than those of odd n above $n = 27$. This suggests an odd-even alternation in cluster stability with respect to the dominant decay process.

(iii) The converse of (i) does not always hold, i.e., for every good (j, k, l) there is not necessarily a local maximum in abundance. The most obvious of these is the (3,5,6) cluster [which would be $\text{Na}_{45}\text{F}_{44}$ and the (5,5,6) cluster ($\text{Na}_{75}\text{F}_{74}$)]. However, these are odd- n clusters, and the fact that they are not a significant local maxima is still consistent with generality (ii). [The last odd- n maximum is $\text{Na}_{27}\text{F}_{26}$, which could be (3,3,6).]

Whereas the level (i) conclusion simply confirms the dominance of cubic lattices, the analysis of levels (ii) and (iii) is not so simple. Perhaps the most naive explanation of the favoritism toward even n can be found by regarding the system as composed of n dipoles (one of which is the Na^+e^- pair), rather than $2n$ ions. [Mathematically, these descriptions are equivalent; conceptually they are not.] Odd- n clusters leave one dipole in the lattice unpaired; even- n clusters can pair all dipoles, so the energy difference for odd versus even cluster evaporation energies is roughly just this pairing energy across the diameter of the cluster. Clearly, this problem deserves further analysis.

C. Electron-attachment-induced isomerization

Landman, Scharf, and Jortner found that, depending upon the depth of the Na pseudopotential used, attachment of an excess electron causes the (1,3,3) planar Na_5Cl_4^+ ion to transform to a pyramidal structure with the electron localized as a diffuse cloud about the tip of the pyramid. Another example of electron-induced isomerization may occur for $\text{Na}_{32}\text{F}_{31}$. For positive ions such as in Fig. 2, we find a relative abundance maximum at $\text{Na}_{32}\text{F}_{31}^+$ suggesting a (3,3,7) cubic ion structure. However, the electron binding energy (estimated to be similar to that of the other *F-center* clusters in that size range), and the neutral abundance of $\text{Na}_{32}\text{F}_{31}^{(0)}$ suggests that it is a (4,4,4) *F-center* cluster with the electron localized in the anion vacancy.

D. Comparison of electron energies with theoretical predictions

Several theoretical methods have been used to make predictions for binding energies of an excess electron interacting with an alkali halide cluster. Different levels of

TABLE II. Comparison of electron binding energies.

	Experiment	<i>F</i> -center model	QUPID (Ref. 13)	MD-FFT (Ref. 12)	Hartree-Fock (Ref. 44)	LDA (Ref. 45)
Na ₂ F	3.85±0.15	3.5		3.47	4.29	
Na ₃ F ₂	3.85±0.15	3.8		3.36		
Na ₄ F ₃	3.54±0.05	4.2		3.27	4.28	
Na ₅ F ₄	3.85±0.15	3.0	4.88		3.80	
Na ₁₄ F ₁₃	1.88±0.05	2.2	1.47	1.81		2.2
Na ₁₈ F ₁₇	2.89±0.05	3.4		2.31		

approximation have been made to make the calculations tractable. Cluster structures are assumed to be crystal-line fragments, or are relaxed simultaneously with the electronic structure, or are sampled from finite-temperature distributions. For comparison between the methods and experiment, Table II shows experimental binding energies and theoretical predictions for several cluster sizes.

The finite-temperature quantum path-integral dynamic (QUPID) simulations of Landman and co-workers¹³ on Na_{*n*}Cl_{*m*} clusters used simplified electron-ion pseudopotentials, and geometries were found simultaneously with the behavior of the excess electron. That study was limited to three clusters, two of which, Na₅Cl₄ and Na₁₄Cl₁₃, were neutral. The general trend of high binding energy for the noncubic cluster, Na₅Cl₄, and low binding energy for the cubic ion, Na₁₄Cl₁₃, is correctly predicted although the electron binding energy is overestimated for Na₅Cl₄ and underestimated for Na₁₄Cl₁₃. Slight differences are expected between the chlorides in that study and the fluorides studied here, which could account for this discrepancy.

The Hartree-Fock results of Pandey, Seel, and Kunz includes several Na_{*n*}F_{*n*-1} clusters.⁴⁴ They find localization properties in good agreement with the earlier LSJ predictions and corroborate our interpretations. Their prediction for the noncubic Na₅F₄ agrees with our experimental classification, and they find a very low electron binding energy for the Li₁₄F₁₃ cubic ion cluster. However, their predictions for Na₂F and Na₄F₃ are substantially higher than the observed values. It was not clear in that work that cluster structures had been fully optimized; this could account for the disagreement with experiment.

Chen *et al.* used first-principles calculational methods based on the local-density approximation (LDA) to study the properties of excess-electron sodium chloride clusters.⁴⁵ They found substantial localization of the excess electron in an anion vacancy such as the corner site in Na₄Cl₃. The excess electron state for the Na₁₄Cl₁₃ cubic structure was found to be delocalized, when cubic symmetry is enforced, resulting in minimal structural reorganization. It was also found to be fairly stable with respect to loss of a neutral sodium atom, requiring 1.74 eV for dissociation. The vertical electron binding energy for Na₁₄Cl₁₃ was calculated to be 2.2 eV, with a very small reorganization energy of the ions. While the excess-electron binding energy is in reasonable agreement with the experimentally observed value for Na₁₄F₁₃, the broad ionization threshold in Fig. 7 suggests substantial reorganization of the cluster ion or temperatures much

higher than those expected from the laser vaporization source.

The results of recent finite temperature, coupled quantum-classical simulations [molecular-dynamics-fast-Fourier transform (MD-FFT)] by Rajagopal *et al.* are also listed in the table.¹² As in the case of clusters without excess electrons, substantially better agreement with experiment was found using interionic interaction potentials from the Born-Huang rather than Fumi-Tosi parameter set. With this choice of interionic potentials, satisfactory agreement with experiment is found for all cluster sizes studied. The adiabatic electron binding energies are close to the observed values, but seem to be systematically underestimated. As discussed above, the significant reorganization energy upon ionization and resultant broad threshold may obscure the adiabatic threshold. For the three largest clusters studied, there is a clear correlation between the reorganization energy E_c and the difference between experiment and theory, ΔE_B . For Na₄F₃ $E_c=0.80$ eV and $\Delta E_B=0.27$ eV; for Na₁₄F₁₃ $E_c=0.21$ eV and $\Delta E_B=0.09$ eV; and finally, for Na₁₈F₁₇ $E_c=1.33$ and $\Delta E_B=0.58$ eV.

E. Localized-electron model

The experimental results and the information from a limited range of quantum calculations motivate a simple model meant to capture the essential physics of the problem and to give quantitative estimates of properties over a wider size range than covered by high-level computations. Even this simple model does not assume a set of structures based on occupation of sites on a cubic lattice, but rather requires that structures and energies have been optimized for each cluster using realistic empirical potentials and annealing. The main assumption of this model is that the excess electron in a M_nX_{n-1} cluster substitutes for the missing anion of a stoichiometric M_nX_n cluster, so that we can use the computed energies of the Na_{*n*}F_{*n*} and Na_{*n*}F_{*n*-1}⁺ clusters from classical simulations to make quantitative predictions of the properties of the excess electron clusters. We have separately provided a complete description of these calculations and results for the cluster sizes of relevance here.³⁴ The optimal structures and energies found for the (NaF)_{*n*} series are shown in Fig. 10. Figure 11 illustrates the relations among the observable and calculated quantities for stoichiometric and excess-electron clusters.

To derive this model, it is first assumed that the electron localizes sufficiently that its contribution to the clus-

ter potential energy is that of a halide ion.⁴⁶ The energy of localizing the electron in a lattice site is its kinetic energy K . In the calculations of LSJ on $\text{Na}_{14}\text{Cl}_{12}^+$, the excess electron localizes in the interior anion vacancy of the cluster, and the zero-temperature kinetic energy of the electron is 1.96 eV.¹³ To scale this for NaF clusters, one can consider the case of an electron localized in a cube of

dimension $2a$. In atomic units $K = 3/8(\pi/a)^2$, so for our estimate we scale the LSJ kinetic-energy value by the square of the ratio of the lattice constants of NaCl to NaF. In this manner, we estimate $K = 2.93$ eV for a $\text{Na}_n\text{F}_{n-1}$ cluster.

Within this model, we can now calculate E_b , the electron binding energy for the ionization process given in

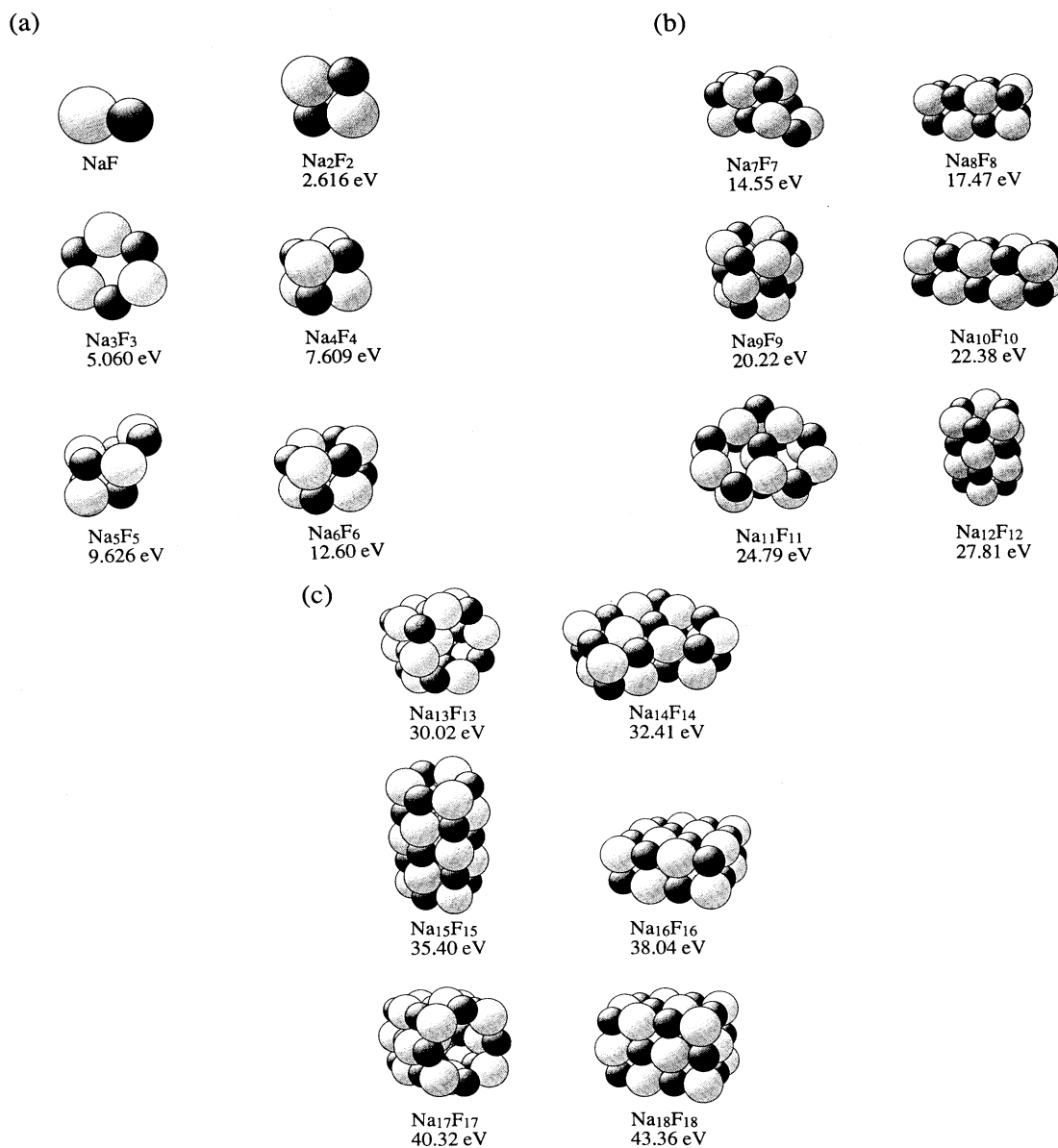


FIG. 10. Optimized structures of $(\text{NaF})_n$ clusters, $n = 1-18$, computed using empirical rigid-ion potentials, from Ref. 32. Small, dark spheres represent Na^+ and large, light spheres represent F^- ions, where the sphere diameters represent the ionic radii. The energies are those calculated for fragmentation into diatomics, $(\text{NaF})_n \rightarrow n \text{NaF}$. Brief description of the structures— $n = 1$: the diatomic; 2: a planar rhombus; 3: a symmetric planar ring, D_{3h} ; 4: cubic (2,2,2), T_d ; 5: a low-symmetry structure (C_2) derived from $n = 4$; 6: two stacked six-membered rings, D_{3d} [a cubic (2,2,3) structure is not topologically distinct from stacked rings, and is slightly higher in energy]; 7: a low-symmetry structure analogous to $n = 5$; 8: cubic (2,2,4), D_{2h} ; 9: three stacked six-membered rings, D_{3h} ; 10: cubic (2,2,5), D_{2h} ; 11: two stacked sheets of low symmetry; 12: four stacked six-membered rings, D_{3d} ; 13: structure derived from the (3,3,3) cube by removal of a face Na^+ , C_{4v} ; 14: two sheets, involving both cubic and ring components; 15: five stacked rings, D_{3h} [the cubic (2,3,5) structure is essentially degenerate to this structure]; 16: cubic (2,4,4), D_{2h} ; structure derived from the (3,3,4) cube by removal of a diatomic (face-interior pair), C_{4v} ; 18: cubic (3,3,4).

Eq. (1), as a function of cluster size,

$$E_b(n) = (E_{n,n} - K) - E_{n,n-1}. \quad (2)$$

Here, $E_{n,n}$ and $E_{n,n-1}$ are the total binding energies from the simulations of the corresponding Na_nF_n and $\text{Na}_n\text{F}_{n-1}^+$ clusters relative to separated ions,³⁴ and K is taken as 2.93 eV as derived above. In accordance with the localization hypothesis, the first quantity in parentheses can be regarded as a proxy for the excess-electron cluster.

The electron binding energies calculated within this model are compared with the experimental values plotted in Fig. 8. While the model does not match the observed binding energies in detail, it does predict the correct magnitude and the very low values for the cubic ion (class I) clusters. In general, it seems to underestimate the binding energies of the noncubic (class III) clusters and overestimate those of the F -center (class II) clusters. A simple pseudopotential for the electron-positive-ion interaction of the form $V(r) = -e^2/r$ ($r > R_c$) and $V(r) = -e^2/R_c$ ($r < R_c$) is only approximated by the F^- ion Na^+ ion interaction for distances larger than R_c . The systematic error therefore, could be indicative of the different modes of electron attachment for the cluster types.¹³

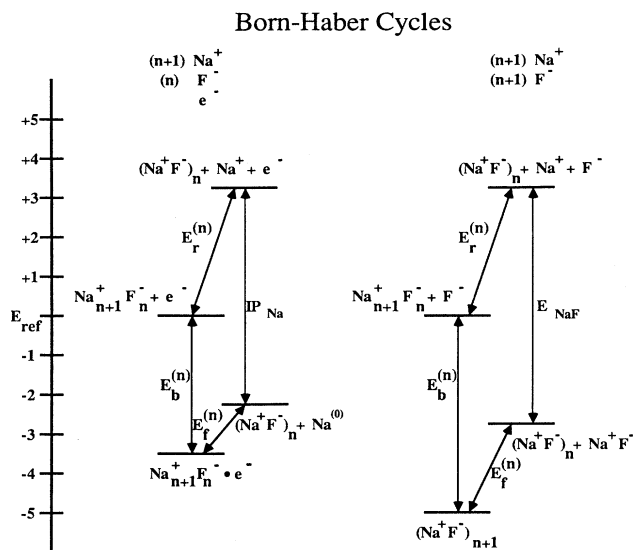
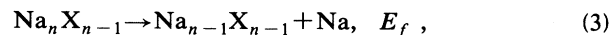


FIG. 11. Thermochemical cycles illustrating the relation between $(\text{NaF})_n$ and $\text{Na}_n\text{F}_{n-1}$ clusters. The energy zero for calculations is with respect to separated ions and excess electrons (see above). The reference energy for comparison of the two cycles can therefore be set equal to the total energies of the separated products $\text{Na}_{n+1}\text{F}_n^+ + e^-$ and $\text{Na}_{n+1}\text{F}_n^+ + \text{F}^-$. At right, the cycle for stoichiometric $(\text{NaF})_{n+1}$, showing the feasible operations, including evaporation of an NaF unit, requiring E_f , and the loss of an F^- ion, requiring E_b . E_{NaF} is the dissociation energy of the diatomic with respect to separated ions. At left, the analogous cycle for $\text{Na}_{n+1}\text{F}_n$, showing the low-energy process of neutral Na atom loss, requiring E_f , and the ionization process, requiring the electron binding energy E_b . IP_{Na} is the ionization energy of the sodium atom.

We can apply this model to the abundance of $\text{Na}_n\text{Cl}_{n-1}$ and $\text{Na}_n\text{F}_{n-1}$ clusters as well. As discussed above, the abundances should be dominated by stability against the fragmentation process



i.e., expulsion of a neutral sodium atom to yield a stoichiometric cluster (undetected), requiring the positive energy E_f . Within the localized electron model, E_f can now be computed from known quantities,

$$E_f^{(n)} = (E_{n,n} - K) - (E_{n-1,n-1} + I_{\text{Na}}). \quad (4)$$

As above, the first term in parentheses is the approximate energy of the excess electron neutral cluster relative to separated ions. The second term, corresponding to the energies of a $\text{Na}_{n-1}\text{F}_{n-1}$ cluster and a neutral Na atom, includes I_{Na} , the ionization potential of the Na atom. (For Na_nCl_n we use the energies calculated by Martin²⁰ and the kinetic-energy value obtained by Landman, Scharf, and Jortner, $K = 1.96$ eV).¹³

The quantity $E_f^{(n)}$ is plotted versus n in Fig. 12 for the two cluster series $\text{Na}_n\text{Cl}_{n-1}$ and $\text{Na}_n\text{F}_{n-1}$. As might be expected from the observed abundances, the pattern is similar in the two series, with E_f ranging from barely positive for clusters such as $n=5$ or 13, to strongly

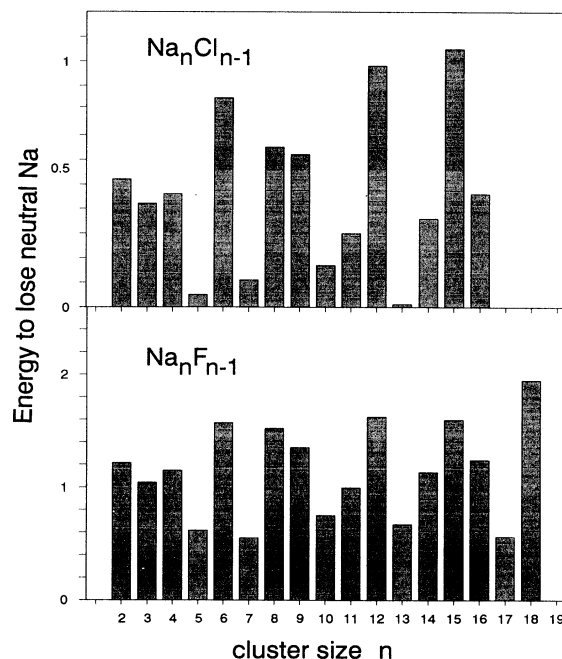


FIG. 12. Energy for neutral $\text{Na}_n\text{Cl}_{n-1}$ and $\text{Na}_n\text{F}_{n-1}$ clusters to fragment to $\text{Na}_{n-1}\text{Cl}_{n-1}$ and $\text{Na}_{n-1}\text{F}_{n-1}$, respectively (undetected), within the electron localization model. Compare the strongly bound sizes to the major peaks in Fig. 3(a). Note also that the ratio between the strongly bound clusters such as Na_6X_5 and the weakly bound Na_5X_4 decreases going from $\text{Na}_n\text{Cl}_{n-1}$ to $\text{Na}_n\text{F}_{n-1}$ as in Fig. 3(a).

bound for $n=6$ or 15. Comparison with Fig. 3 shows very good agreement with the clusters having a large fragmentation energy being relatively abundant and those with a small fragmentation energy being much weaker, if present at all.

In addition to the good agreement within each $\text{Na}_n\text{X}_{n-1}$ series, the model also provides an explanation for the difference between the abundances of the $\text{Na}_n\text{Cl}_{n-1}$, $\text{Na}_n\text{F}_{n-1}$, and $\text{Li}_n\text{F}_{n-1}$ clusters. As seen in Fig. 4, the ratio between the abundant F -center clusters (such as M_6X_5) and the less abundant noncubic clusters (such as M_5X_4) decreases going from $\text{Na}_n\text{Cl}_{n-1}$ to $\text{Li}_n\text{F}_{n-1}$. A correspondence is seen in Fig. 12 where the ratio of the fragmentation energies between the strongly and weakly bound clusters also decreases in going from $\text{Na}_n\text{Cl}_{n-1}$ to $\text{Na}_n\text{F}_{n-1}$. This can be qualitatively understood by the increased energy of localizing the electron in a lattice site as the lattice constant decreases. In going from NaCl to LiF, the energy of localizing the electron increases until it competes with the potential energy gained from the electron being in the anion vacancy, resulting in only a slight stability enhancement for the F -center (class II) $\text{Li}_n\text{F}_{n-1}$ clusters.

The success of this model demonstrates that the excess electron tends to localize in the cluster. When the electron can occupy a site that completes a cuboid structure, this implies high cluster stability (with respect to atom expulsion) and strong electron binding. The most stable among these are j , k , and l nearly equal. When such a site is not possible, the electron occupies a site in the non-cuboid cluster, resulting in somewhat higher electron binding (at least in the vertical sense) but very low stability, as reflected in abundances. Finally, if the cluster is an odd cuboid, its excess-electron state is very weakly bound relative to its symmetrical ionized state, and it will also be somewhat unstable.

V. CONCLUSIONS

We have presented experimental evidence for a wide range of excess-electron-dominated behavior in alkali halide clusters. This rich behavior in a comparatively simple, finite-size system may provide further insight into a range of problems involving electron localization and solvation. We have described a simple model of electron localization which is consistent with the main features of the experimental observations, but the nature of these systems makes them ideal candidates for advanced theoretical methods involving coupled quantum and classical degrees of freedom.

The optical spectra of the excess-electron clusters have provided for continued systematic comparison between experiment and theory. Pioneering work in this direction has been undertaken by Kappes and co-workers, who found transitions in the blue-green region for the triatomic Na_2Cl .⁴² Using resonant two-photon ionization, we have found strong absorption bands for the $\text{Na}_n\text{F}_{n-1}$ clusters ($n=2-15$) in the yellow-red and near-infrared regions, with the F -center and noncubic clusters each displaying unique optical spectra.^{12,47} Aside from further establishing the nature of the excess-electron ground state, several other directions can be envisaged, including the study of the metal-insulator transition, other structural transitions, and melting.

ACKNOWLEDGMENTS

The authors are indebted to Dr. Pierre Labastie and Dr. Kenneth E. Schriver for assistance in the early stages of these experiments. Funding was provided by the Office of Naval Research and the UCLA Solid State Science Center. R.L.W. acknowledges financial support from the NSF and the Packard Foundation. M.L.H. would like to thank UCLA for funding.

*Also at Physics Department, UCLA. Present address: AT&T Bell Laboratories, Murray Hill, NJ 07974.

¹*Elemental and Molecular Clusters*, edited by G. Benedek, T. P. Martin, and G. Pacchioni (Springer-Verlag, Berlin, 1988).

²*Physics and Chemistry of Small Clusters*, edited by P. Jean, B. K. Rao, and S. N. Khanna (Plenum, New York, 1987).

³*Small Particles and Inorganic Clusters*, edited by Olof Echt and Ekkehard Recknagel (Springer-Verlag, Berlin, 1991).

⁴P. P. Edwards and M. J. Sienko, *Acc. Chem. Res.* **15**, 87 (1982); *Physics and Chemistry of Electrons and Ions in Condensed Matter*, Vol. 130 of *NATO Advanced Study Institute Series C: Mathematical and Physical Sciences*, edited by J. V. Acrivos, N. F. Mott, and A. D. Yoffe (D. Reidel, Dordrecht, 1983); pp. 287-436; F. Hensel and H. Uchtmann, *Ann. Rev. Phys. Chem.* **40**, 61 (1989).

⁵W. D. Knight, K. Clemenger, W. A. de Heer, W. A. Saunders, M. Y. Chou, and M. L. Cohen, *Phys. Rev. Lett.* **52**, 2141 (1984); W. D. Knight, W. A. de Heer, K. Clemenger, and W. A. Saunders, *Solid State Commun.* **53**, 445 (1985).

⁶S. Pollack, C. R. C. Wang, and M. M. Kappes, *Z. Phys. D* **12**, 241 (1989).

⁷T. Bergmann, H. Limberger, and T. P. Martin, *Phys. Rev. Lett.* **60**, 1767 (1988); H. G. Limberger and T. P. Martin, *J. Chem.*

Phys. **90**, 2979 (1989); T. Bergmann and T. P. Martin, *ibid.* **90**, 2848 (1989); H. G. Limberger and T. P. Martin, *Z. Phys. D* **12**, 439 (1989).

⁸A. Wallqvist, D. Thirumalai, and B. J. Berne, *J. Chem. Phys.* **85**, 1583 (1986); R. N. Barnett, U. Landman, and A. Nitzan, *Phys. Rev. Lett.* **62**, 106 (1989).

⁹M. Sprik, R. W. Impey, and M. L. Klein, *J. Chem. Phys.* **83**, 5802 (1985); P. Stampfli and K. H. Bennemann, *Phys. Rev. Lett.* **58**, 2635 (1987); R. N. Barnett, U. Landman, and A. Nitzan, *J. Chem. Phys.* **91**, 5567 (1989).

¹⁰P. Stampfli and K. H. Bennemann, *Phys. Rev. A* **38**, 4431 (1988); G. J. Martyna and B. J. Berne, *J. Chem. Phys.* **90**, 3744 (1989).

¹¹G. Rajagopal, R. N. Barnett, and U. Landman, *Phys. Rev. Lett.* **67**, 727 (1991).

¹²G. Rajagopal, R. N. Barnett, A. Nitzan, U. Landman, E. C. Honea, P. Labastie, M. L. Homer, and R. L. Whetten, *Phys. Rev. Lett.* **64**, 2933 (1990).

¹³U. Landman, D. Scharf, and J. Jortner, *Phys. Rev. Lett.* **54**, 1860 (1985); R. N. Barnett, U. Landman, D. Scharf, and J. Jortner, *Acc. Chem. Res.* **22**, 350 (1989); See also, J. Jortner, D. Scharf, and U. Landman, in *Elemental and Molecular Clusters*, edited by G. Benedek, T. P. Martin, and G. Pac-

- chioni (Springer-Verlag, Berlin, 1989), pp. 169–189; D. Scharf, J. Jortner, and U. Landman, *J. Chem. Phys.* **87**, 2716 (1987).
- ¹⁴C. E. Klots and R. N. Compton, *J. Chem. Phys.* **69**, 1644 (1978); H. Haberland, C. Ludewigt, H.-G. Schindler, and D. R. Worsnop, *J. Phys. Chem.* **81**, 3742 (1984); M. Knapp, O. Echt, D. Kreisle, and E. Recknagel, *ibid.* **91**, 2601 (1987); L. A. Posey, P. J. Campagnola, M. A. Johnson, G. H. Lee, J. G. Eaton, and K. H. Bowen, *J. Chem. Phys.* **91**, 6536 (1989); H. Haberland, T. Kolar, and T. Reiners, *Phys. Rev. Lett.* **63**, 1219 (1989).
- ¹⁵E. C. Honea, M. L. Homer, P. Labastie, and R. L. Whetten, *Phys. Rev. Lett.* **63**, 394 (1989).
- ¹⁶E. C. Honea, M. L. Homer, and R. L. Whetten, *Int. J. Mass Spectrosc. Ion Proc.* **102**, 213 (1990).
- ¹⁷Y. A. Yang, C. W. S. Conover, and L. A. Bloomfield, *Chem. Phys. Lett.* **158**, 279 (1989); T. M. Miller and W. C. Lineberger, *Int. J. Mass Spectrosc. Ion Proc.* **102**, 239 (1990); P. Xia, A. J. Cox, Y. A. Yang, and L. A. Bloomfield, in *Physics and Chemistry of Finite Systems: From Clusters to Crystals, Vol. II*, Vol. 374 of *NATO Advanced Study Institute, Series C: Mathematical and Physical Sciences*, edited by P. Jena, S. N. Khanna, and B. K. Rao (Kluwer, Dordrecht, 1992), pp. 1019–1024.
- ¹⁸Y. A. Yang, L. A. Bloomfield, C. Jin, L. S. Wang, and R. E. Smalley, *J. Chem. Phys.* **96**, 2453 (1992).
- ¹⁹T. P. Martin, *Phys. Rev. B* **15**, 4071 (1977).
- ²⁰T. P. Martin, *Phys. Rep.* **95**, 167 (1983), and references therein.
- ²¹F. Honda, G. M. Lancaster, U. Fukuda, and J. W. Rabalais, *J. Chem. Phys.* **69**, 4931 (1978).
- ²²J. E. Campana, T. M. Barlak, R. J. Colton, J. J. DeCorpo, J. R. Wyatt, and B. I. Dunlap, *Phys. Rev. Lett.* **47**, 1046 (1981); T. M. Barlak, J. R. Wyatt, R. J. Colton, J. J. DeCorpo, and J. E. Campana, *J. Am. Chem. Soc.* **104**, 1212 (1982).
- ²³T. M. Barlak, J. E. Campana, J. R. Wyatt, B. I. Dunlap, and R. J. Colton, *Int. J. Mass Spectrosc. Ion Proc.* **46**, 523 (1983).
- ²⁴W. Ens, R. Beavis, and K. G. Standing, *Phys. Rev. Lett.* **50**, 27 (1983).
- ²⁵R. Pflaum, P. Pfau, K. Sattler, and E. Recknagel, *Surf. Sci.* **156**, 165 (1985); R. Pflaum, K. Sattler, and E. Recknagel, in *Physics and Chemistry of Small Clusters*, edited by P. Jena, B. K. Rao, and S. N. Khanna (Plenum, New York, 1987), pp. 103–108; R. Pflaum and E. Recknagel, *Z. Phys. D* **12**, 249 (1989).
- ²⁶H. J. Hwang, D. K. Sensharma, and M. A. El-Sayed, *J. Phys. Chem.* **93**, 5012 (1989); *Chem. Phys. Lett.* **160**, 243 (1989).
- ²⁷J. J. Markham, *F-centers in Alkali Halides* (Academic, New York, 1966).
- ²⁸K. S. Pitzer, *J. Am. Chem. Soc.* **84**, 2025 (1962); M. Parrinello and A. Rahman, *J. Chem. Phys.* **80**, 860 (1984); W. W. Warren, Jr., B. F. Campbell, and G. F. Brennert, *Phys. Rev. Lett.* **58**, 941 (1987); W. Freyland, K. Garbade, and E. Pfeiffer, *ibid.* **51**, 1304 (1983).
- ²⁹A. Selloni, P. Carnevali, R. Car, and M. Parrinello, *Phys. Rev. Lett.* **59**, 823 (1986).
- ³⁰A. N. H. Nachtrieb, *Adv. Chem. Phys.* **31**, 465 (1975).
- ³¹R. T. Williams, R. M. Wilson, and J. Liu, *Nucl. Instrum. Methods Phys. Res. B* **65**, 473 (1992).
- ³²E. Matthias, H. B. Nielsen, J. Reif, A. Rosén, and E. Westin, *J. Vac. Sci. Technol. B* **5**, 1415 (1987).
- ³³A. C. Roach and M. S. Child, *Mol. Phys.* **14**, 1 (1961); S. M. Lin, J. G. Wharton, and R. Grice, *ibid.* **26**, 317 (1973); W. S. Struve, *ibid.* **25**, 777 (1973); G. Galli, W. Andreoni, and M. P. Tosi, *Phys. Rev. A* **34**, 3580 (1986).
- ³⁴M. L. Homer (unpublished).
- ³⁵R. E. Smalley, *Laser Chem.* **2**, 167 (1983); J. G. Dietz, M. A. Duncan, D. E. Powers, and R. E. Smalley, *J. Chem. Phys.* **74**, 6511 (1981); V. E. Bondybey, and J. H. English, *J. Phys. Chem.* **74**, 6978 (1981).
- ³⁶E. C. Honea, M. L. Homer, J. L. Persson, and R. L. Whetten, *Chem. Phys. Lett.* **171**, 147 (1990).
- ³⁷M. L. Homer, J. L. Persson, E. C. Honea, and R. L. Whetten, *Z. Phys. D* **22**, 441 (1991).
- ³⁸C. W. S. Conover, Y. A. Yang, and L. A. Bloomfield, *Phys. Rev. B* **38**, 3517 (1988); Y. J. Twu, C. W. S. Conover, Y. A. Yang, and L. A. Bloomfield, *ibid.* **42**, 5306 (1990).
- ³⁹One of the most abundant species detected under these conditions is the alkali halide carbon complex $\text{Na}_{14}\text{Cl}_{12}\text{C}$. Given the cubic structure of $\text{Na}_{14}\text{Cl}_{13}$, an immediate structure which comes to mind is that of a central C atom surrounded by a cubic cage of $\text{Na}_{14}\text{Cl}_{12}$. Sulfur from SF_6 is also incorporated into certain cluster sizes as well. The cubic clusters $\text{Na}_{38}\text{F}_{36}\text{S}$ and $\text{Na}_{63}\text{F}_{61}\text{S}$ are relatively abundant S-containing species observed using 5.0-eV photoionization.
- ⁴⁰K. I. Peterson, P. D. Dao, and A. W. Castleman, Jr., *J. Chem. Phys.* **79**, 777 (1983); M. M. Kappes, P. Radi, M. Schär, and E. Schumacher, *Chem. Phys. Lett.* **113**, 243 (1985).
- ⁴¹J. E. Eby, K. J. Teegarden, and D. B. Dutton, *Phys. Rev.* **116**, 1099 (1959).
- ⁴²S. Pollack, C. R. C. Wang, and M. M. Kappes, *Chem. Phys. Lett.* **175**, 209 (1990).
- ⁴³I. Tamm, *Z. Phys.* **76**, 849 (1932); N. F. Mott and R. W. Gurney, *Electronic Processes in Ionic Crystals*, 2nd ed. (Clarendon, Oxford, 1948), p. 86.
- ⁴⁴R. Pandey, M. Seel, and A. B. Kunz, *Phys. Rev. B* **41**, 7955 (1990); R. Pandey, X. Yang, J. M. Vail, and J. Zuo, *Solid State Commun.* **81**, 549 (1992).
- ⁴⁵J. L. Chen, C. W. Wang, K. A. Jackson, and M. R. Pederson, *Phys. Rev. B* **45**, 1927 (1992).
- ⁴⁶Another simple model has been used to explain the electron affinities of alkali-halide diatomics, involving a highly polarized Na atom; T. M. Miller, D. G. Leopold, K. K. Murray, and W. C. Lineberger, *J. Chem. Phys.* **85**, 2368 (1986).
- ⁴⁷E. C. Honea, Ph.D. thesis, UCLA, 1990; E. C. Honea *et al.* (unpublished).